nature climate change

SUPPLEMENTARY INFORMATION

DOI: 10.1038/NCLIMATE2196

Land management and land-cover change have impacts of similar magnitude on surface temperature

Supplementary Online Material:

1 Defining land cover and land management

2 Materials and Methods

3 State of the art of biophysical effects of land management

Figures 1-4

Tables 1-5

References (89)

Supplementary Materials:

1 Defining land cover and land management

In our study, we compared the effects on surface climate from changes in land surface properties that arise from land cover changes (LCC) to those that arise from land management change (LMC) that does not involve a change in land cover (Table 1). Land cover is defined as “the attributes of the Earth’s land surface and immediate subsurface, including biota, soil, topography, surface and groundwater, and human (mainly built-up) structures.” Where applicable we adopted the following definitions [1]: Land-cover changes – also called land cover conversion – constitute the replacement of one cover type by another and are measured by a shift from one land-cover category, such as a specific vegetation type, to another. Land cover change thus occurs, e.g., due to expansion of croplands, deforestation, or a change in urban extent [1]. Land cover changes can occur naturally, as happened throughout Earth's history when the vegetation cover adjusted to changing orbital parameters, or it can be an indirect cause of anthropogenic disturbances such as human-induced climate change. In our study, however, we adopt the term “land cover change” only for direct anthropogenic land cover changes which are driven by changes in land use, where land use is the “purpose for which humans exploit the land cover”. In this study land cover changes includes changes between forest, grassland and croplands.

In contrast to land cover change, land management refers to the “ways in which humans treat vegetation, soil, and water” for a specific purpose. Examples are the use of fertilizers and pesticides, irrigation for mechanized cultivation in drylands, the use of an introduced grass species for pasture, the tree species used in reforestation and the sequence of moving livestock in a ranching system [1]. Thus, although we restricted the spatial extent of our definition of land management to the area affected by human activities but having not experienced land cover change, changes in land management can occur on land that either has or has not been subject to land cover change.

While land cover change usually leads to a change in land surface properties, e.g., “changes in biotic diversity, actual and potential primary productivity, soil quality, runoff and sedimentation rates, and other such attributes of the terrestrial surface of the Earth”, land management does not necessarily induce large changes in land surface properties (e.g. fertilization). The data analyzed in our study shows, however, that the climatic consequences of the change in land surface properties from land management are often on the same order of magnitude as those from land cover change.

In our study, we count neither the conversion of an unmanaged, natural grassland to a managed, grazed grassland (pasture) nor the conversion of natural forest to tree plantation as land cover change. Although these conversions are clearly driven by a change in land use and frequently subsumed under land cover change in climate modeling studies, in most cases it does not represent an actual change in vegetation type.

2 Materials and methods

2.1 Regional effects of land cover and land management change

Cross-border areas provide interesting natural experiments to isolate the effect of land management on land surface properties in cases where political borders dissect environmentally homogeneous regions [2–5]. We selected eleven such cross-border regions, consisting of three regions where countries differed in terms of land cover changes (e.g., forest on one side of the border and deforestation on the other side), and five regions where land cover was similar but land management differed (e.g., high grazing pressure on one side of the border and low grazing pressure on the other). For testing our approach, we applied the same method to three additional regions where land cover and land management were assumed to be homogeneous (Table 4).

2.1.1 Data

We acquired time series of MODIS land surface temperature, black sky albedo, and the enhanced vegetation index from the NASA Land Processes Distributed Active Archive Centre (LP DAAC, https://lpdaac.usgs.gov). Regarding surface temperature, we used the product MOD11A2 (collection 5), acquired by the Terra satellite (both morning and evening passes) at a spatial resolution of 1 km. Land surface temperature is derived using a generalized split-window algorithm [6] and MOD11A2 represents the average values of clear-sky land surface temperatures during an 8-day period. For a detailed algorithm description of this product, we refer to the 'Collection-5 MODIS Land Surface Temperature Products' and the 'MODIS Land-Surface Temperature Algorithm Theoretical Basis Document (LST ATBD) Version 3.3' available from the product page of LP DAAC (https://lpdaac.usgs.gov/products/modis_products_table/mod11a2).

Regarding black sky albedo, we used the combined product of the Aqua (overpass time: 1:30 pm) and Terra satellites (MCD43B3, collection 5), at a spatial resolution of 1 km. Black sky albedo refers to the directional hemispherical reflectance at local solar noon and is estimated using the RossThick-LiSparseReciprocal Bidirectional reflectance distribution function (BRDF) model that describes the anisotropy of reflectance of each pixel [7,8]. The black sky albedo is calculated for the three broad bands visible (VIS), near-infrared (NIR), and shortwave (SW) using a spectral-to-broadband conversion based on the three visible, four near-infrared, or all of these bands, respectively. Since the

MCD43B3 product uses data from both MODIS satellites, a higher data quality is achieved than using a single sensor alone. The MCD43B3 represents the average of all clear-sky observation over a 16-day period. For a detailed algorithm description of this product, we refer to the 'Collection-5 MODIS BRDF/Albedo Product (MOD43B) User's Guide' and the 'MODIS BRDF/Albedo Product: Algorithm Theoretical Basis Document Version 5.0' available from the product page of LP DAAC (https://lpdaac.usgs.gov/products/modis_products_table/mcd43b3)

We used the Enhanced Vegetation Index (EVI) in the MOD13A2 product from the Terra product at a spatial resolution of 1 km (collection 5) as a proxy for leaf cover. The Enhanced Vegetation Index (EVI) is an improved version of the Normalized Difference Vegetation index and integrates the red, near-infrared, and blue band of the MODIS sensor to minimizes canopy background variations and maintains sensitivity over dense vegetation conditions [9]. For a detailed algorithm description of this product, we refer to the 'MODIS Vegetation Index User's Guide (MOD13 Series)' and the 'MODIS Vegetation Index (MOD 13) Algorithm Theoretical Basis Document Version 3' available from the product page of LP DAAC (https://lpdaac.usgs.gov/products/modis_products_table/mod13a2).

We also used the MODIS Land Water Mask (MOD44W, spatial resolution of 250m), which is based on integrating Shuttle Radar Topography Mission (SRTM) data and MODIS land surface reflectance data. For a detailed algorithm description of this product, we refer to the University of Maryland (UMD) Global 250 m Land Water Mask User Guide (https://lpdaac.usgs.gov/products/modis_products_table/mod44w).

2.1.2 Pre-processing the MODIS time series

For each cross-border region we selected a 50 x 50 km^2 area bisected by the administrative border. We buffered the border by 5 km on each side of the border and excluded all MODIS pixels within this buffer to avoid uncertainty due to spatial misalignment of the MODIS images and the political boundary spatial layers. We masked all water pixels from the analyses and all areas with an EVI value lower than 0.01. Furthermore, we excluded all pixels where EVI data quality was flagged as poor and excluded all pixels with values outside the valid land surface temperature range (i.e., <7,500 or >65,535, see User's Guide), and excluded all pixels with values outside the valid albedo range (i.e., 0-32,276). Further, a Savitzky–Golay filter [10] was applied to the land surface temperature and albedo time series to reduce the noise in our time series and to correct for outliers. We used the time series software package TIMESAT [11]□ for the filtering. Finally, we identified the timing of peak vegetation for each site and averaged the land surface temperatures and the albedo values for the month containing the vegetation peak for the three years 2009-2011 per pixel using the software TimeStats [12]□.

2.1.3 Calculation cross-border differences in land surface temperature and albedo

We randomly selected 1,000 pixel pairs consisting of one observation from each side of the border. Each pixel was allowed to enter multiple pairs in this procedure. The three homogenous sites were subdivided into two equally sized sub-regions assuming a perpendicular border. We then calculated the absolute difference in land surface temperature and albedo per pixel pair, and the average and standard error differences for land surface temperature and albedo for each site (standard error for albedo is not shown).

The upper limit temperature response to LCC and LMC is similar and around 6 K at the site-level (Fig. 2A) and up to 4 K at the regional scale (Fig. 2B). Note that many individual MODIS pixel comparisons differed by 6 K or more (Fig. 2), such that the difference in effect between the site and regional analysis can partly be explained by the different scales of observations between the two data sets [13]□.

2.2 Biophysical effects of land cover and land management change

2.2.1 The energy budget

Energy conservation requires that at the site-level the incoming energy flux equals the sum of the outgoing energy flux and the energy stored in the biomass. Focusing on the dominant terms of the energy budget, and thus ignoring small fluxes at the daily time scale such as energy used in photosynthesis and stored in biomass and the subcanopy air space, the energy balance at the site can be written as:

$$Rn = \lambda E + H + G \qquad (1)$$

where λE, H and G refer to respectively the latent heat flux, the sensible heat flux and the soil heat flux all expressed in W m^{-2}. Rn is the net radiation absorbed by the land surface (W m^{-2}) and equals the sum of the incoming shortwave Rsi (W m^{-2}) and the incoming longwave radiation Rli (W m^{-2}), minus the loss from reflected shortwave Rso (W m^{-2}) and emitted longwave radiation Rlo (W m^{-2}). The outgoing shortwave radiation is a function of the incoming radiation and albedo (α). The outgoing longwave radiation is emitted by the surface and is given by the Stefan-Boltzmann law and thus depends on radiometric surface temperature (Ts), the Stefan-Boltzmann constant constant (σ) and emissivity (ε). Rn can then be written as:

$$Rn = (1-\alpha)Rsi + Rli - \varepsilon\sigma Ts^4 \qquad (2)$$

The method used in this study to decompose the surface temperature signal into its major components was adapted from Juang et al. [14] but also extended to allow for comparisons of sites with different incoming radiation. When the approach is used with site-level observations, measurement errors and our simplifications need to be accounted for. This was done by adding a residual 'imbalance' flux denoted by I (W m^{-2}). The residual flux thus includes: the error due to neglecting photosynthetic fluxes, the error due to neglecting heat storage in the biomass and atmosphere, and systematic errors and random errors from measuring radiative and energy fluxes. When accounting for these methodological issues, equation 2 is completed as:

$$(1-\alpha)Rsi + Rli - \varepsilon\sigma Ts^4 = \lambda E + H + G + I \qquad (3)$$

and eq. 3 can be rearranged to obtain the surface temperature:

$$\varepsilon\sigma Ts^4 = (1-\alpha)Rsi + Rli - \lambda E - H - G - I \qquad (4)$$

When using an energy budget approach (eq. 4), surface temperature (Ts) is the straightforward choice as a metric for temperature. The choice for radiative surface temperature implies that the analysis takes an ecosystem [15]□ rather than a climate perspective (as explored in §2.2.3 and §2.2.4) and that the analysis can be complemented by the land surface temperature product from MODIS.

2.2.2 Energy budget decomposition

One of the strengths of the decomposition approach is that it quantifies the net effect of dynamic responses. For example when LMC decreases LAI, soil heat flux will likely increase which results in less available energy for latent and sensible heat fluxes following eq. 1, if all else remains constant, although the change in LAI will alter Rn depending on the albedo and surface temperature of the modified surface. The net effect of the decrease in LAI is captured by the decomposition approach. However, the decomposition approach used here does not allow us to quantify the gross fluxes for the above example: how much of the change in latent heat is due to the change in LAI [16]□, how much is due to the change in net radiation and how much is due to the change in the temperature gradient between the canopy and the atmosphere.

The left hand side (LHS) of eq. 4 is a function of Ts and ε: LHS = $f_L(\text{Ts}, \varepsilon)$. The right hand side (RHS) is a function of seven parameters: RHS = f_R□(α, Rsi, Rli, λE, H, G, I). The only constant parameter is σ. The changes in the energy budget from changes in the land surface can be formalized as the first order derivative of the LHS of eq. 4, excluding higher order terms:

$d f_L = (\partial f_L/\partial \varepsilon)\Delta\varepsilon + (\partial f_L/\partial \text{Ts})\Delta\text{Ts}$

where $\partial f_L/\partial\varepsilon = \sigma \text{Ts}^4$ and $\partial f_L/\partial \text{Ts} = 4\varepsilon\sigma\text{Ts}^3$

and the first order derivative of the RHS of eq. 4:

$d f_R = (\partial f_R/\partial\alpha)\Delta\alpha + (\partial f_R/\partial \text{Rsi})\Delta\text{Rsi} + (\partial f_R/\partial \text{Rli})\Delta\text{Rli} + (\partial f_R/\partial \lambda\text{E})\Delta\lambda\text{E} + (\partial f_R/\partial \text{H})\Delta\text{H} + (\partial f_R/\partial \text{G})\Delta\text{G} + (\partial f_R/\partial \text{I})\Delta\text{I}$

where $\partial f_R/\partial\alpha = -\text{Rsi}$, $\partial f_R/\partial\text{Rsi} = (1-\alpha)$, $\partial f_R/\partial\text{Rli} = 1$, $\partial f_R/\partial\lambda\text{E} = -1$, $\partial f_R/\partial\text{H} = -1$, $\partial f_R/\partial\text{G} = -1$ and $\partial f_R/\partial\text{I} = -1$.

Since $d f_{\mathrm{L}} = \mathrm{d} f_R$, $\sigma Ts^4\Delta\varepsilon+4\varepsilon\sigma Ts^3\Delta Ts = -Rsi\Delta\alpha+\square(1-\alpha)\Delta Rsi+\Delta Rli-\Delta\lambda E-\Delta H-\Delta G-\Delta I$. Hence, the expression for discrete changes of ΔTs (K) due to land cover change or land management change consists of eight terms:

$$\Delta Ts= (4\varepsilon\sigma Ts^3)^{-1}\square\{-Rsi\Delta\alpha+\square(1-\alpha)\Delta Rsi+\Delta Rli-\Delta\lambda E-\Delta H-\Delta G-\Delta I-\sigma Ts^4\Delta\varepsilon\}$$

(5)

I II III IV V VI VII VIII

This decomposition is applied to each pair of observational sites (Table 3). The symbol Δ represents the difference between the two sites for each of the variables. From equation 5, we can attribute the change in surface temperature due to the eight factors, following land cover change or land management change:

I. ΔTs due to a change in albedo: a positive ΔTs for this term implies that following land cover change the albedo decreases (the changed surface is darker) and that more incident shortwave radiation is absorbed by the surface as a consequence;

II. ΔTs due to a change in Rsi: if the new land cover receives more incoming shortwave radiation than the initial land cover, ΔTs will be positive for this component;

III. ΔTs due to a change in Rli: a positive ΔTs for this component represents an increase in incoming longwave radiation from the atmosphere;

IV. ΔTs due to a change in latent heat flux: a positive ΔTs indicates a change in cooling due to decreases in λE, that is to say that the new land cover/management has less evaporative cooling than the original land cover/management;

V. ΔTs due to a change in sensible heat flux: as IV;

VI. ΔTs due to a difference in soil heat flux: as IV;

VII. ΔTs due to the residual flux: given that I combines unmeasured fluxes and measurement errors of the observed fluxes, we cannot separate it to determine the error from the missing components. Nevertheless, the magnitude of this flux was used as a threshold to interpret ΔTs resulting from the other components; site pairs are only presented if the fluxes of interest are larger than the imbalance term (see also §2.2.4).

VIII. ΔTs due to a change in the thermal emissivity of the surface. A positive ΔTs due to $\Delta\varepsilon$

means that the new land cover emits more outgoing longwave radiation due to its higher emissivity coefficient, which results in a higher Ts.

Excluding the nine pairs from formal experimental ecosystem set-ups, the remaining 33 pairs had (slightly) different radiative regimes. Hence, a change in all of the components of the eq. 4 is to be anticipated, including incoming shortwave and incoming longwave radiation. The extended decomposition approach [14,16] applied in this study differs from previous decomposition approaches in that it accounts for differences in incoming radiation and quantifies an imbalance term containing all measurement errors including all issues with energy balance closure. The lack of a significant relationship between the major components of the energy budget and the observed imbalance (Fig. 3) suggests that despite simplifications in Eq. 4 and the measurement errors and uncertainties, the main results of this study are not driven by the imbalance term. Where ΔTs is reported in the manuscript this is calculated as the sum of $\Delta Ts\alpha$, $\Delta Ts\lambda E$, ΔTsH and ΔTsG .

2.2.3 Boundary layer height

Extending the analysis toward the planetary boundary layer (PBL) strengthens its climate perspective, within the limits of the simple PBL model used here [17,18]. The observed sensible and latent heat fluxes of the vegetated surface were coupled to a 1D boundary layer model [19] that is expressed in virtual or equivalent heat flux, thus coupling the latent and sensible components in a single coherent framework. For climate impact, this is a much more realistic metric than only surface or atmospheric temperature [20]. The change in height in the boundary layer (Δh, in m) over a time step Δt (s) is given in this model as:

$$\Delta h = (H_v \, \Delta t) / (\rho_a \, c_p \, h \, \gamma_v) \qquad (6)$$

where ρ_a is the air density in kg m^{-3}, c_p is the specific heat capacity in J kg^{-1} K^{-1}, h is the current height of the boundary layer in m, γ_v is the virtual temperature inversion strength in K m^{-1}, and H_v is the virtual heat flux (W m^{-2}) and is calculated from the observed sensible (W m^{-2}) and latent heat fluxes (W m^{-2}) as follows:

$$H_v = H + 0.07\lambda E \qquad (7)$$

At the start of each day the initial height of the boundary layer (h) was set to 150 m and γ_v was kept constant at 0.003 K m^{-1} as observed at Oak Ridge, TN for selected days during 1999 (personal communication Dennis Baldocchi).

2.2.4 Equivalent temperature

The change in partial pressure of water vapour (ΔP_v, Pa) in the boundary layer is given by

$$\Delta P_v = \Delta t\ \lambda E\ /\ (h\ \rho_a\ \epsilon\ \lambda/P_d) \tag{8}$$

where T_a is the atmospheric temperature of the boundary layer (K), ϵ is the mass of vapor to dry air ratio and P_d is the dry air partial pressure of the boundary layer (Pa). λ is the latent heat of vaporization (J kg^{-1}), which is estimated by the temperature function

$\lambda = 3149000 - 2370\ T_a$.

For consistency, P_d was kept constant at 101300 Pa. The specific humidity in (kg kg^{-1}), may be expressed as [21]□:

$$q_v = (\epsilon\ (P_v + \Delta P_v))\ /\ (P_d + \epsilon\ (P_v + \Delta P_v)) \tag{9}$$

and the equivalent temperature (T_E) of the atmosphere (K) is given by Fall et al. [20]□:

$$T_E = T_a + \lambda(q_v/c_p) \tag{10}$$

Irrespective of whether surface or boundary layer temperature is being investigated, quantifying the full climate effects of LMC and LCC at the annual scale is out of reach for site-level observations. Such an approach would require coupled surface-atmosphere models to account for boundary layer dynamics, planetary albedo from clouds and aerosols, convective and frontal precipitation, and radiative forcing from changes in atmospheric composition through aerosols, C and N cycling. Nevertheless, a joint analysis of the major components of the ecosystem energy budget in PBL models contributes to understanding the first order biophysical effects of LMC.

2.2.5 Observations used for surface temperature decomposition

Site measurements over different European and American terrestrial ecosystems were used for attributing changes in surface temperature to the different underlying processes. The measurements used in our study were obtained from principal site investigators and the network-based databases

FLUXNET, IMECC[22] and AMERIFLUX. Although this collection of sites lacks a formal design and harmonized site-level methodology, all sites are equipped with an eddy covariance system to continuously monitor half-hourly land-atmosphere fluxes of CO_2, water and energy. In this analysis H and λE measurements from the eddy covariance system were used. All other measurements were retrieved from additional sensors to monitor other meteorological variables such as the incident and outgoing shortwave and longwave radiation fluxes and air temperature.

Despite the attention paid to quality issues, uncertainties and errors are inherent to any experimental approach. In this study, the most important sources of uncertainty are:
(a) Random error, which is inherent to any measurement and, in the case of eddy-covariance measurements, is associated to unpredictable fluctuations in atmospheric turbulence. This uncertainty tends to be small (5%) when aggregated at the annual scale[23].
(b) Systematic bias, due to for example a change in sensors, can often be identified and corrected. Other systematic errors are expected but hard to quantify, i.e., the effect of wet sensors following rain events.
(c) Gaps in the long-term dataset, resulting from meteorological events affecting operation of the tower such as storms. Other causes of data-gaps are sensor breakdown, maintenance periods, dirty sensors, etc. Even good eddy-covariance based time series may contain up to 40% gaps on an annual scale[24].
(d) Energy balance closure is most likely the main source of uncertainty in this analysis and we therefore elaborate on this issue in the following paragraphs (§2.2.7).

2.2.6 Site selection

Nine sites, marked with * in Table 2, are part of a formal experimental set-up in which the environmental conditions were deliberately sought to be similar and the vegetation different. When paired, these sites resulted in two experiments studying land cover change and seven experiments studying land management (marked with * in Table 3). The rest of the site data comes from an ad-hoc monitoring network that lacks formal experimental design. Consequently, the available sites were rearranged in pseudo-experiments to mimic an experimental set-up of land cover change and land management change. The pseudo-experiment introduced here simulates a succession of different vegetation types, where space substitutes for time. The pseudo-experiments become more powerful if the sites used in the experiment are similar in all respects except for the factor under study. This approach allows us to examine the effects of land cover change and land management on land-atmosphere interactions.

We included all forest, grasslands, cropland and peatland sites for which all variables required for the energy balance decomposition approach were observed. Furthermore, to rule out potential artifacts with latitude, altitude and inter-annual variability, sites were only paired in pseudo-experiments if the following criteria were satisfied:
(a) the pair represented a possible land cover change or land management change (i.e., sites on mineral and organic soils were not paired)
(b) the sites within a pair were located on a similar latitude (i.e., within 5° latitude from each other)
(c) the sites within a pair were located on the same continent (i.e., European and US sites were not paired)
(d) the sites had a small imbalance term compared to other components of the energy budget (i.e., the contribution of H, LE or albedo had to be larger than the contribution of the imbalance term to change in radiometric surface temperature)
(e) the sites within a pair had at least one common year of measurements. The decomposition was only made when temporal overlap occurred. Hence, the number of years included in this study is less than the number of available years.

Applying these criteria, 22 sites (Table 3) were selected and combined into 33 pairs (Table 4) out of the 351 possible pairs. Sites can be paired in two ways, i.e., A-B and B-A. For one pair ΔTs will be positive, for the other pair ΔTs will be negative. For land cover changes, the order of the sites within a pair was determined by the cover change, i.e., forest to grassland. In this case we only included data for forest to grass land and did not include the data for grassland to forest. For land management changes, we presented only one randomly selected combination for each pair. Where useful (i.e., Fig. 2a) we used the modulus of ΔTs. Whenever the modulus resulted in a sign change of ΔTs, all eight terms of decomposition were multiplied by -1.

Despite the effort made and care taken in site selection, the observed differences between sites in the pseudo-experiments can only be partly attributed to different management as differences in environmental conditions could not be entirely excluded. However, since this effect plays for both, pairs representing land cover changes and for land management changes, we reasoned that our key messages were not affected by this as they rely on a comparison of land cover changes against land management changes.

2.2.7 Data post-processing

A typical data set contained, for several years, quality checked half-hourly energy fluxes and related meteorological data. To be used in the proposed ΔTs decomposition approach, the data required post-processing to deal with additional data quality issues (a-d) and to derive additional variables (e-h):

(a) Half-hourly measurements were averaged to apply the decomposition at a daily resolution. A filter was applied to retain only days for which both day and night observations were present in order to obtain a representative daily mean. Twenty four hour periods with more than 66% of nighttime or 66% of daytime measurements missing were discarded.

(b) The residual imbalance flux, I, was computed daily, since the assumptions underlying equation 3 are more likely to be valid at daily time scale. Days with unreliable measurements were removed according to the following procedure. A regression analysis between (Rn-G) and (H+λE) was performed to estimate values of I, which was detrended to remove the seasonal pattern. All days for which the detrended values exceeded the 95% confidence interval of the detrended standard deviation were removed from the analysis.

(c) A filter was applied to remove outliers irrespective of their cause. For each time series, the high and low threshold values were defined as the first and third quartiles. Values 1.5 times above or below the thresholds were considered as outliers and discarded from the time series

(d) Only original observations were used in this analysis. Following the application of all the above-mentioned filters to the different variables needed for this study, the remaining time series were rather rich in gaps. To have a fully consistent comparison between the sites pairs the gaps from one site in the pair were introduced in the other site.

(e) Surface albedo was computed as the ratio of outgoing shortwave solar radiation to incident shortwave solar radiation. During the day, α is not constant because it depends on the solar zenith angle. α is a minimum near mid-day, when the solar zenith angle is the smallest. As a result, α for this study was averaged from mid-day (10:00-13:00) solar radiation measurements, in order to avoid bias due to a too low solar angle on the sensor. This averaged α was then used as the surface albedo value for the entire day. The same time slot was used to calculate the ratio of latent heat over net radiation (λE/Rn), sensible heat over net radiation (H/Rn) and the Bowen ratio (H/λE).

(f) Since there was no direct measurement of the emissivity coefficient of the vegetation, an empirical relationship between α and ε, reported by Juang et al.[14]□, was used to compute ε values for each day: $\varepsilon = - 0.16\,\alpha + 0.99$, $R^2 = 0.94$. This relationship was computed from literature reporting α and ε measurements for crops and forests in temperate regions.

(g) To have measured ΔTs to compare with our calculated ΔTs (Equation 5), the radiometric temperature Ts was calculated at a half-hourly time scale from outgoing longwave radiation measurements, following the Stefan-Boltzmann law (see eq. 2). It should be noted that the requirement of outgoing longwave radiation measurements to compute the radiative temperature of the vegetation cover largely limited the number of available sites for our study.

(h) Finally, site observations were compared and decomposed at the daily time-step, and the mean of the daily decomposition values was used in this study. The measured ΔTs was used as a quality criteria: the calculated ΔTs should have the same sign and be of the same magnitude as the measured ΔTs for the decomposed budget to be accepted.

2.3 Spatial extent of global land cover changes, land management and wilderness areas in 2000 (Table 1 and Fig. 3)

The spatial extent of land cover changes in Fig. 4 is based on Pongratz et al. [25]. It represents all changes in natural vegetation cover due to expansion of cropland and pasture, except for conversion of natural grassland to pasture, which is assumed not to constitute a change in vegetation cover type.

The spatial extent of wilderness and non-productive areas (derived from Haberl et al. [26], based on the human footprint dataset [27] and a model run with the dynamic vegetation model LPJ) is estimated to represent 32-37 Mkm^2, or 24-28% of the 130 Mkm^2 of ice-free land surface of the Earth. In the absence of spatially explicit land management maps, the remainder (93-98 Mkm^2) were considered as being affected by human activities, either through land cover change or land management without conversion (land modification), following the definitions above. Consequently, this number pools extensively managed areas, e.g., hunting reserves, occasionally grazed lands or extensively used forests with intensively managed lands, such as high-input croplands. This takes into account that annually harvested forest areas are – by their rotation period – integrated in a much larger area subject to the same forestry regime, and that extensive grazing systems are found across most biomes.

The global extent of the main land cover changes – towards built-up and cropland areas, and forest being converted to pastures – for 2000 were estimated from various sources (Table 1). In total, 23-38 Mkm^2 were thus affected by land cover change in 2000, or 18-29% of the ice-free land surface. The remainder of the non-wilderness and productive areas (55-75 Mkm^2 or 42-58% of the ice-free land surface) was potentially affected by land management to various degrees.

3 State of the art of biophysical effects of land management

In forests, strategies with low thinning volumes, for example, tend to result in lower albedo values in the visible range [28]. Forests also become darker with age due to changes in canopy structure [29,30] and forest albedo partly depends on species composition [28,31]. Although the mechanism is still being debated, leaf nitrogen concentrations correlate to the albedo of closed canopies; hence, management strategies refraining from nitrogen fertilization have been found to have a lower surface albedo than strategies applying fertilization [32]. Recent findings have attributed the observed relationship between albedo and canopy N to changes in canopy structure, which still impacts the surface roughness [33].

The effects of cropland and grassland management on their surface biophysics are manifold (Table 5). Among the more intrusive changes is the conversion from cropland or grassland into greenhouses, which doubles the albedo on average [34]. Irrigation enhances actual evapotranspiration and thus latent heat flux until potential evapotranspiration has been reached [35]. Furthermore, evapotranspiration depends on soil water holding capacity, which in turn is affected by tillage [36] and crop residue management [37]. More productive cultivars and earlier planting dates affect energy partitioning; due to the shorter growing season, dark soil is exposed sooner resulting in a lower end-of-season albedo [38]. Whether the end-of-season albedo increases or decreases depends on the ratio between the soil and vegetation albedo. In many regions of the world soil albedo is lower than plant albedo, but this is not the case for, e.g., some (semi-)arid regions where soils may have a similar or even higher albedo than the vegetation. Furthermore, fertilization is expected to increase plant albedo [32] and simultaneously decrease the canopy albedo because of enhanced canopy cover. Frequent grazing and mowing have been reported to lower surface albedo at less intensively grazed sites during rainy seasons due to higher vegetation cover [39–41]. However, the effect of grazing and mowing on albedo is likely to depend on soil albedo as well, since very intensive grazing and mowing is likely to expose more soil.

Peatlands contribute little to satisfy the human demand for food, fiber, and fuel until drained for peat mining and/or to enhance plant productivity [42]. This lowering of the water table is a key driver for the biophysical changes associated with land cover change on peatlands (Table 5). The magnitude and direction of the changes in albedo, evapotranspiration, sensible heat, and surface roughness depends on the nutrient status of the undrained mire or fen [43], the new level of the lowered groundwater table [44–46] and whether the new land cover consists of crops or trees, the two primary uses of drained peatlands.

Supplementary references

1. Lambin, E. F., Geist, H. & Rindfuss, R. R. in *Land-Use Land-Cover Chang.* (Lambin, E. F. & Geist, H.) 1–8 (Springer-Verlag, 2006).
2. Homewood, K. *et al.* Long-term changes in Serengeti-Mara wildebeest and land cover: Pastoralism, population, or policies? *Proc. Natl. Acad. Sci. U. S. A.* **98,** 12544–12549 (2001).
3. Kuemmerle, T., Hostert, P., Radeloff, V. C., van der Linden, S. Perzanowski, K. & Kruhlov, I. Cross-border comparison of post-socialist farmland abandonment in the Carpathians. *Ecosystems* **11,** 614–628 (2008).
4. Kuemmerle, T., Hostert, P., Perzanowski, K. & Radeloff, V. C. Cross-border comparison of land cover and landscape pattern in Eastern Europe using a hybrid classification technique. *Remote Sens. Environ.* **103,** 449–464 (2006).
5. Soto-Berelov, M. & Madsen, K. Continuity and Distinction in Land Cover Across a Rural Stretch of the U.S.-Mexico Border. *Hum. Ecol.* **39,** 509–526 (2011).
6. Wan, Z. & Dozier, J. A generalized split-window algorithm for retrieving land-surface temperature from space. *IEEE Trans. Geosci. Remote Sens.* **34,** 892–905 (1996).
7. Lucht, W., Schaaf, C. B. & Strahler, A. H. An Algorithm for the retrieval of albedo from space using semiempirical BRDF models. *IEEE Trans. Geosci. Remote Sens.* **38,** 977–998 (2000).
8. Schaaf, C. B. *et al.* First operational BRDF, albedo nadir reflectance products from MODIS. *Remote Sens. Environ.* **83,** 135–148 (2002).
9. Huete, A. *et al.* Overview of the radiometric and biophysical performance of the MODIS vegetation indices. *Remote Sens. Environ.* **83,** 195–213 (2002).
10. Chen, J. *et al.* A simple method for reconstructing a high-quality NDVI time-series data set based on the Savitzky–Golay filter. *Remote Sens. Environ.* **91,** 332–344 (2004).
11. Jönsson, P. & Eklundh, L. TIMESAT - a program for analyzing time-series of satellite sensor data. *Comput. Geosci.* **30,** 833–845 (2004).
12. Udelhoven, T. TimeStats: A Software Tool for the Retrieval of Temporal Patterns From Global Satellite Archives. *IEEE J. Sel. Top. Appl. Earth Obs. Remote Sens.* **4,** 310–317 (2011).
13. Cescatti, A. *et al.* Intercomparison of MODIS albedo retrievals and in situ measurements across the global FLUXNET network. *Remote Sens. Environ.* **121,** 323–334 (2012).
14. Juang, J.-Y. Y., Katul, G., Siqueira, M., Stoy, P. & Novick, K. A. Separating the effects of albedo from eco-physiological changes on surface temperature along a successional chronosequence in the southeastern United States. *Geophys. Res. Lett.* **34,** 1–5 (2007).
15. Rotenberg, E. & Yakir, D. Distinct patterns of changes in surface energy budget associated with forestation in the semiarid region. *Glob. Chang. Biol.* **17,** 1536–1548 (2011).
16. Stoy, P. C. *et al.* Separating the effects of climate and vegetation on evapotranspiration along a successional chronosequence in the southeastern US. *Glob. Chang. Biol.* **12,** 2115–2135 (2006).
17. Lee, X. *et al.* Observed increase in local cooling effect of deforestation at higher latitudes. *Nature* **479,** 384–387 (2011).
18. Baldocchi, D. D. & Ma, S. How will land use affect air temperature in the surface boundary layer?

Lessons learned from a comparative study on the energy balance of an oak savanna and annual grassland in California, USA. *Tellus B* **65,** in press (2013).

19. McNaughton, K. G. & Spriggs, T. W. A mixed-layer model for regional evaporation. *Boundary-Layer Meteorol.* **34,** 243–262 (1986).
20. Fall, S., Diffenbaugh, N. S., Niyogi, D., Pielke, R. a. & Rochon, G. Temperature and equivalent temperature over the United States (1979-2005). *Int. J. Climatol.* **30,** 2045–2054 (2010).
21. Jacobson, M. Z. *Fundamentals of Atmospheric Modeling*. (Cambridge University Press, 2005).
22. IMECC-CO2NRT. Infrastructure for Measurement of the European Carbon Cycle Near real time processing of atmospheric CO_2 data. (2008). at <http://www.imecc.org>
23. Richardson, A. D. *et al.* A multi-site analysis of random error in tower-based measurements of carbon and energy fluxes. *Agric. For. Meteorol.* **136,** 1–18 (2006).
24. Moffat, A. J. M. *et al.* Comprehensive comparison of gap-filling techniques for eddy covariance net carbon fluxes. *Agric. For. Meteorol.* **147,** 209–232 (2007).
25. Pongratz, J., Reick, C., Raddatz, T. & Claussen, M. A reconstruction of global agricultural areas and land cover for the last millennium. *Global Biogeochem. Cycles* **22,** 16 (2008).
26. Erb, K.-H. *et al.* A comprehensive global 5 min resolution land-use data set for the year 2000 consistent with national census data. *J. Land Use Sci.* **2,** 191 (2007).
27. Sanderson, E. W. *et al.* The Human Footprint and the Last of the Wild. *BioSciences* **52,** 891–904 (2002).
28. Otto, J. *et al.* Summertime canopy albedo is sensitive to forest thinning. *Biogeosciences Discuss.* (2013).
29. Rautiainen, M., Stenberg, P., Mottus, M. & Manninen, T. Radiative transfer simulations link boreal forest structure and shortwave albedo. *Boreal Environ. Res.* **16,** 91–100 (2011).
30. Amiro, B. D. D. *et al.* The effect of post-fire stand age on the boreal forest energy balance. *Agric. For. Meteorol.* **140,** 41–50 (2006).
31. Hollinger, D. Y. *et al.* Albedo estimates for land surface models and support for a new paradigm based on foliage nitrogen concentration. *Glob. Chang. Biol.* **16,** 696–710 (2010).
32. Wicklein, H. F. *et al.* Variation in foliar nitrogen and albedo in response to nitrogen fertilization and elevated CO_2. *Oecologia* **169,** 915–925 (2012).
33. Knyazikhin, Y. *et al.* Hyperspectral remote sensing of foliar nitrogen content. *Proc. Natl. Acad. Sci. U. S. A.* **110,** E185–92 (2013).
34. Muñoz, I., Campra, P. & Fernández-Alba, A. R. Including CO_2-emission equivalence of changes in land surface albedo in life cycle assessment. Methodology and case study on greenhouse agriculture. *Int. J. Life Cycle Assess.* **15,** 672–681 (2010).
35. Payero, J. O., Tarkalson, D. D., Irmak, S., Davison, D. & Petersen, J. L. Effect of irrigation amounts applied with subsurface drip irrigation on corn evapotranspiration, yield, water use efficiency, and dry matter production in a semiarid climate. *Agric. Water Manag.* **95,** 895–908 (2008).
36. Cresswell, H. P., Painter, D. J. & Cameron, K. C. Tillage and water content effects on surface

hydraulic properties and shortwave albedo. *Soil Sci. Soc. Am. J.* **57,** 816–824 (1993).

37. Horton, R., Bristow, K. L., Kluitenberg, G. J. & Sauer, T. J. Crop residue effects on surface radiation and energy balance — review. *Theor. Appl. Climatol.* **54,** 27–37 (1996).
38. Sacks, W. J. & Kucharik, C. J. Crop management and phenology trends in the U.S. Corn Belt: Impacts on yields, evapotranspiration and energy balance. *Agric. For. Meteorol.* **151,** 882–894 (2011).
39. Fan, L., Ketzer, B., Liu, H. & Bernhofer, C. Grazing effects on seasonal dynamics and interannual variabilities of spectral reflectance in semi-arid grassland in Inner Mongolia. *Plant Soil* **340,** 169–180 (2011).
40. Rosset, M., Montani, M., Tanner, M. & Fuhrer, J. Effects of abandonment on the energy balance and evapotranspiration of wet subalpine grassland. *Agric. Ecosyst. Environ.* **86,** 277–286 (2001).
41. Li, S. G. *et al.* Grassland desertification by grazing and the resulting micrometeorological changes in Inner Mongolia. *Agric. For. Meteorol.* **102,** 125–137 (2000).
42. Laine, J., Laiho, R., Minkkinen, K. & Vasander, H. in *Boreal Peatl. Ecosyst.* (Wieder, R. K. & Vitt, D. H.) (Springer-Verlag, 2006).
43. Lohila, A. *et al.* Forestation of boreal peatlands: Impacts of changing albedo and greenhouse gas fluxes on radiative forcing. *J. Geophys. Res.* **115,** 1–15 (2010).
44. Wu, J., Kutzbach, L., Jager, D., Wille, C. & Wilmking, M. Evapotranspiration dynamics in a boreal peatland and its impact on the water and energy balance. *J. Geophys. Res.* **115,** G04038 (2010).
45. Marshall, C. H., Pielke, R. A. & Steyaert, L. T. Crop freezes and land-use change in Florida. *Nature* **426,** 29–30 (2003).
46. Schwärzel, K., Simunek, J., van Genuchten, M. T. T., Wessolek, G. & Šimůnek, J. Measurement and modeling of soil-water dynamics and evapotranspiration of drained peatland soils. *J. Plant Nutr. Soil Sci. Fur Pflanzenernahrung Und Bodenkd.* **169,** 762–774 (2006).
47. Cho, J. *et al.* Testing the hypothesis on the relationship between aerodynamic roughness length and albedo using vegetation structure parameters. *Int. J. Biometeorol.* **56,** 411–8 (2012).
48. FAO. *Global Forest Resources Assessment 2010*. 378 (Food and Agriculture Organization of the United Nations, 2010).
49. Hansen, M. C., Stehman, S. V & Potapov, P. V. Quantification of global gross forest cover loss. *Proc. Natl. Acad. Sci. U. S. A.* **107,** 8650–5 (2010).
50. Schneider, A., Friedl, A. M. & Potere, D. A new map of global urban extent from MODIS satellite data. *Environ. Res. Lett.* **4,** 044003 (2009).
51. CIESIN, IFPRI & CIAT. *Global Rural-Urban Mapping Project (GRUMP)*. (2005). at <http://sedac.ciesin.columbia.edu/data/collection/gpw-v3>
52. Ramankutty, N. & Foley, J. Estimating historical changes in global land cover: Croplands from 1700 to 1992. *Global Biogeochem. Cycles* **13,** 997–1027 (1999).
53. FAO. FAOSTAT. *faostat.fao.org* (2012).
54. Ramankutty, N., Evan, A. T., Monfreda, C. & Foley, J. A. Farming the planet: 1. Geographic distribution of global agricultural lands in the year 2000. *Global Biogeochem. Cycles* **22,**

GB002952 (2008).

55. Béziat, P., Ceschia, E. & Dedieu, G. Carbon balance of a three crop succession over two cropland sites in South West France. *Agric. For. Meteorol.* **149,** 1628–1645 (2009).

56. Stella, P. *et al.* Simultaneous measurements of CO_2 and water exchanges over three agroecosystems in South-West France. *Biogeosciences* **6,** 2957–2971 (2009).

57. Allard, V., Ourcival, J. M., Rambal, S., Joffre, R. & Rocheteau, A. Seasonal and annual variation of carbon exchange in an evergreen Mediterranean forest in southern France. *Glob. Chang. Biol.* **14,** 714–725 (2008).

58. Jacobs, C. M. J. *et al.* Variability of annual CO_2 exchange from Dutch grasslands. *Biogeosciences* **4,** 803–816 (2007).

59. Hendriks, D. M. D., van Huissteden, J., Dolman, A. J. & van der Molen, M. K. The full greenhouse gas balance of an abandoned peat meadow. *Biogeosciences* **4,** 411–424 (2007).

60. Moors, E. J. *Water Use of Forests in the Netherlands, Alterra Scientific Contributions 41*. 290 (2012). at <http://dare.ubvu.vu.nl/handle/1871/33480>

61. Novick, K. A. *et al.* Carbon dioxide and water vapor exchange in a warm temperate grassland. *Oecologia* **138,** 259–274 (2004).

62. Op de Beeck, M. *et al.* Needle age-related and seasonal photosynthetic capacity variation is negligible for modelling yearly gas exchange of a sparse temperate Scots pine forest. *Biogeosciences* **7,** 199–215 (2010).

63. Dore, S. *et al.* Carbon and water fluxes from ponderosa pine forests disturbed by wildfire and thinning. *Ecol. Appl.* **20,** 663–83 (2010).

64. Suyker, A. E., Verma, S. B., Burba, G. G. & Arkebauer, T. J. Gross primary production and ecosystem respiration of irrigated maize and irrigated soybean during a growing season. *Agric. For. Meteorol.* **131,** 180–190 (2005).

65. Knohl, A., Schulze, E.-D. D., Kolle, O. & Buchmann, N. Large carbon uptake by an unmanaged 250-year-old deciduous forest in Central Germany. *Agric. For. Meteorol.* **118,** 151–167 (2003).

66. Don, A., Rebmann, C., Kolle, O., Scherer-Lorenzen, M. & Schulze, E.-D. Impact of afforestation-associated management changes on the carbon balance of grassland. *Glob. Chang. Biol.* **15,** 1990–2002 (2009).

67. Grünwald, T. & Bernhofer, C. A decade of carbon, water and energy flux measurements of an old spruce forest at the Anchor Station Tharandt. *Tellus B* **59,** 387–396 (2007).

68. Rebmann, C. *et al.* Treatment and assessment of the CO_2-exchange at a complex forest site in Thuringia, Germany. *Agric. For. Meteorol.* **150,** 684–691 (2010).

69. Pilegaard, K., Ibrom, A., Courtney, M. S., Hummelshøj, P. & Jensen, N. O. Increasing net CO2 uptake by a Danish beech forest during the period from 1996 to 2009. *Agric. For. Meteorol.* **151,** 934–946 (2011).

70. Lohila, A. *et al.* Carbon dioxide exchange above a 30-year-old Scots pine plantation established on organic-soil cropland. *Boreal Environ. Res.* 141–157 (2007). at <http://cat.inist.fr/?aModele=afficheN&cpsidt=18767562>

71. Lohila, A., Aurela, M., Tuovinen, J.-P. & Laurila, T. Annual CO_2 exchange of a peat field growing spring barley or perennial forage grass. *J. Geophys. Res.* **109,** D18116 (2004).

72. Rosset, M., Riedo, M. & Grub, A. Seasonal variation in radiation and energy balances of permanent pastures at different altitudes. *Agric. For. Meteorol.* **86,** 245–258 (1997).

73. Hammerle, A., Haslwanter, A., Tappeiner, U., Cernusca, A. & Wohlfahrt, G. Leaf area controls on energy partitioning of a temperate mountain grassland. *Biogeosciences* **5,** 421–431 (2008).

74. Wang, S. & Davidson, A. Impact of climate variations on surface albedo of a temperate grassland. *Agric. For. Meteorol.* **142,** 133–142 (2007).

75. Genesio, L. *et al.* Surface albedo following biochar application in durum wheat. *Environ. Res. Lett.* **7,** 014025 (2012).

76. Rose, L., Coners, H. & Leuschner, C. Effects of fertilization and cutting frequency on the water balance of a temperate grassland. *Ecohydrology* **5,** 64–72 (2012).

77. Ford, C. R., Laseter, S. H., Swank, W. T. & Vose, J. M. Can forest management be used to sustain water-based ecosystem services in the face of climate change? *Ecol. Appl.* **21,** 2049–67 (2011).

78. Lafleur, P. M., Hember, R. A., Admiral, S. W. & Roulet, N. T. Annual and seasonal variability in evapotranspiration and water table at a shrub-covered bog in southern Ontario, Canada. *Hydrol. Process.* **19,** 3533–3550 (2005).

79. Petrone, R. M., Price, J. S., Waddington, J. M. & von Waldow, H. Surface moisture and energy exchange from a restored peatland, Québec, Canada. *J. Hydrol.* **295,** 198–210 (2004).

80. Miller, S. D. *et al.* Reduced impact logging minimally alters tropical rainforest carbon and energy exchange. *Proc. Natl. Acad. Sci. U. S. A.* **108,** 19431–5 (2011).

81. Venäläinen, A., Rontu, L. & Solantie, R. On the influence of peatland draining on local climate. *Boreal Environ. Res.* **4,** 89–100 (1999).

82. Boucher, O., Myhre, G. & Myhre, A. Direct human influence of irrigation on atmospheric water vapour and climate. *Clim. Dyn.* **22,** 597–603 (2004).

83. Montes-Helu, M. C. *et al.* Persistent effects of fire-induced vegetation change on energy partitioning and evapotranspiration in ponderosa pine forests. *Agric. For. Meteorol.* **149,** 491–500 (2009).

84. Rambal, S., Lacaze, B. & Winkel, T. Testing an area-weighted model for albedo or surface temperature of mixed pixels in Mediterranean woodlands. *Int. J. Remote Sens.* **11,** 1495–1499 (1990).

85. Bussière, F. & Cellier, P. Modification of the soil temperature and water content regimes by a crop residue mulch: experiment and modelling. *Agric. For. Meteorol.* **68,** 1–28 (1994).

86. Anda, A. & Løke, Z. Radiation Balance Components of Maize Hybrids Grown at Various Plant Densities. *J. Agron. Crop Sci.* **209,** 202–209 (2005).

87. Eastman, J. L. J., Coughenour, M. B. & Pielke, R. A. Does grazing affect regional climate? *J. Hydrometeorelogy* **2,** 243–253 (2001).

88. Amiro, B. Paired-tower measurements of carbon and energy fluxes following disturbance in the boreal forest. *Glob. Chang. Biol.* **7,** (2001).

89. Ogunjemiyo, S., Parker, G. & Roberts, D. Reflections in Bumpy Terrain: Implications of Canopy Surface Variations for the Radiation Balance of Vegetation. *IEEE Geosci. Remote Sens. Lett.* **2,** 90–93 (2005).

Figure captions

Figure 1. Site location and site pairs. Land cover change (LCC) pairs are shown in blue and land management (LMC) pairs are shown in red. The background shows the ecoregions.

Figure 2. Cumulative probability density function of the absolute difference in surface temperature between site observations (n=33; black) and individual MODIS pixels (n=11,000; gray). The two data sources have a similar probability density function.

Figure 3. **Relationship between the total energy budget imbalance (I) and the major components of the energy budget**. The lack of a significant relationship between the major components of the energy budget and the observed imbalance suggests that despite the simplifications, measurement errors and uncertainties, the main results of the analysis are not driven by the imbalance term. **a,** Relationship between measured change in radiative surface temperature and the change in the energy imbalance ($p > 0.14$). **b**, Relationship between the change in surface temperature due to a change in albedo and the change in temperature due to a change in energy imbalance ($p > 0.38$). **c**, Relationship between the change in surface temperature due to a change in latent heat flux and the change in energy imbalance ($p > 0.77$). **d**, Relationship between the change in surface temperature due to a change in sensible heat flux and the change in energy imbalance ($p > 0.31$).

Figure 4. **Relationship between canopy structure and albedo, sensible, and latent heat fluxes**. Green markers represent forest, yellow markers grassland and blue markers cropland. Sites from formal experiments are marked with a diamond and all other sites are marked with a square. Cho et al. [47]□ established a convincing relationship between roughness length and the logarithm of the ratio of height over LAI. Given that roughness length is available for only half of the sites, the aforementioned proxy was used in the analysis. **a**, Relationship between the proxy for roughness and albedo ($p < 0.01$), suggesting that both surface characteristics are at least partly controlled by canopy composition, structure and density. Changes in canopy structure due to land cover change or land management change will affect both the albedo and roughness length. **b**, The proxy for roughness relates to the ratio of the net radiation to sensible heat (H/Rn) (slope = 0.08, $p < 0.01$). **c**, However, a change in roughness is not related to a change in $\lambda E/Rn$ (slope = -0.04, $p = 0.16$). Subplots b and c suggest that H is more

sensitive to changes in roughness than λE.

Table 1. Global land use and land management in 2000. Absolute (Mkm^2) and relative (% of ice-free land surface) land surface area of different types of land cover changes and land management.

Land cover type	**Surface area (Mkm^2)**		**Surface area(%)**		**Comments**
	Low	**High**	**Low**	**High**	
Total ice-free land	130.4	130.4	100.0	100.0	
Urban / built-up	0.7	3.5	0.5	2.7	Low and high esitimates are based on refs. [50] and [51]
Cropland, total	15.1	18.8	11.6	14.4	Low estimates are based on ref. [53], proportions of original land cover from ref. [26], high estimates based based on ref. [52,25].
on forest	7.9	10.8	6.1	8.2	
on natural grassland and savannah	5.3	5.9	4.1	4.5	
on shrub and tundra	1.9	2.1	1.5	1.6	
Pasture, total	28.0	34.1	21.5	26.2	Low [54], proportions of original land cover from refs. [25,53], proportions of original land cover based on ref. [26].
on forest	3.1	8.3	2.4	6.4	

on natural grassland and savannah	18.3	20.5	14.0	15.7	
on shrub and tundra	4.3	7.5	3.3	5.8	
Forests under use, total	26.5	29.4	20.3	22.6	Sum of the sub-categories
Planted forests	2.2	2.2	1.6	1.6	Based on ref. [48]□
semi-natural planted forests	0.9	0.9	0.7	0.7	
industrial plantations	1.3	1.3	1.0	1.0	
Human-modified natural forests	24.4	27.3	18.7	20.9	Low based on ref. [49]□, total forest area, minus planted forests from ref. [48]□ and forested wilderness from ref. [26]□; Highbased on ref. [48]□.
affected by logging / used for forestry	19.1	19.1	14.7	14.7	FAO 2010, production plus multiple uses (which includes forestry) forests.
affected by other uses	5.2	8.1	4.0	6.2	Difference between the two above.
Wilderness and non-productive land, total	32.0	37.2	24.5	28.5	Low estimated based on ref. [26]□. High based on ref. [26]□ with primary forest from ref. [48]□
non-productive, including snow	16.2	16.2	12.4	12.4	Based on ref. [25]
productive wilderness, forested	6.2	11.4	4.7	8.7	Low estimate based on ref. [26]□. High based on ref. [48]□

productive wilderness, unforested	9.6	9.6	7.4	7.4	Based on ref. [25].
Other land affected by management / human activities (unforested, productive land)	7.4	28.1	5.7	21.6	Residual. This includes savannah, woodlands, and other vegetation, some being used for extensive and seasonal grazing.
Total land cover change	**23.2**	**38.1**	**17.8**	**29.2**	Sum of urban and built-up, cropland, and pastures sourced from forests, shrubs and tundra.
Total land management without land cover change	**55.1**	**75.2**	**42.3**	**57.7**	Sum of pastures sourced from natural grasslands and savannah, forests under use, and other land affected by land management.
Total wilderness	**32.0**	**37.2**	**24.5**	**28.5**	Low estimate based on ref. [26]; High based on ref. [26] with primary forest from ref. [48].

Table 2. Site characteristics of the observational sites used in this study. M: mineral soil; O: organic soil; Bh: boreal humid; Bsa: boreal semi-arid; Th: temperate humid; Tsd: temperate summer dry; B: broadleaved; N: needle-leaved; D: deciduous; E: evergreen; LAI: projected leaf area index. Budyko index as a proxy for water availability. Height: maximum canopy height during the growing season; z0: roughness length of the canopy; α: shortwave albedo; H/λE: Bowen ratio calculated as the ratio of H over λE; λE/Rn: energy efficiency for latent heat calculated as the ratio of λE over net radiation (Rn); H/Rn: energy efficiency for sensible heat calculated as the ratio of H over net Rn. * indicates that the sites are part of an experimental set-up, † intra-annual variability, ‡ inter-annual variability and ∫ spatial variability within a site. Leaf area index, canopy height and roughness length are based on literature and personal communication with the principal investigators of the sites.

Site name	**Cover type**	**Description**	**Species**	**LAI (-)**	**Budyko (-)**	**Height (m)**	**z0 (m)**	**α (-)**	**H/λE (-)**	**λE/Rn (-)**	**H/Rn (-)**	**Ref.**
BE-Bra	Forest	M/Th/N, E	*Pinus sylvestris* L.	1.3	1.1	18	1.0	0.08	1.80	0.20	0.38	[62]
DE-Hai	Forest	M/Th/B, D	*Fagus sylvatica* L., Fraxinus excelsior L.	6.0	1.0	33	3.2	0.10	1.22	0.30	0.36	[65]
DE-Meh	Grassland	M/Th	*Trisetum flavescens* P. Beauv.	0.8-2.4†	0.9	0.5	0.03	0.17	1.82	0.17	0.28	[66]
DE-Tha	Forest	M/Th/N, E	*Picea abies* L.	7.5	1.3	27	2.3	0.07	1.77	0.24	0.41	[67]
DE-Wet	Forest	M/Th/N, E	*Picea abies* L.	7.0	1.1	22		0.05	2.46	0.17	0.37	[68]
DK-Sor	Forest	M/Th/B, D	*Fagus sylvatica* L.	4.9	0.9	25	1.8	0.14	1.00	0.33	0.23	[69]

FI-Alk	Forest on peat	O/Bh, N, E	*Pinus sylvestris* L.	3.6	-	12	1.4	0.18	1.07	0.44	0.49	[70]
FI-Jok	Cropland on peat	O/Bh	*Hordeum vulgare* L.	5.9	-	0.7	0.04	0.40	0.86	0.29	0.26	[71]
*FR-Aur	Cropland	M/Th	*Brassica napus* L. *Triticum aestivum* L., *Helianthus annuus* L. and *Triticum aestivum* L.	0.7-1.7‡	1.3	0.7-4‡		0.16	0.81	0.34	0.28	[55]
*FR-Lam	Cropland	M/Th	*Triticosecale, Zea mays* L. and *Triticum aestivum* L.	0.9-2.5‡	1.5	0.7-3‡		0.16	0.90	0.37	0.27	[55]
FR-LBr	Forest	M/Th, N, E	*Pinus pinaster* Ait.	4.7	1.3	21	1.6	0.11	1.25	0.30	0.37	[56]
FR-Pue	Forest	M/Tsd, B, E	*Quercus ilex* L.	2.8	1.5	6	0.5	0.12	2.79	0.17	0.44	[57]
NL-Ca1	Grassland	M/Th	*Lolium perenne* L.	3.0	1.0	0.3		0.23	0.25	0.50	0.13	[58]
NL-Hor	Grassland	O/Th	*Phragmites*		1.0	0.2-2∫	0.04	0.17	0.36	0.52	0.24	[59]

			australis (Cav.) Trin. ex Steud., *Holcus lanatus* L., *Agrostis stolonifera* L.									
NL-Loo	Forest	M/Th, N, E	*Pinus sylvestris* L.	3.3	1.3	16	2.5	0.09	0.93	0.35	0.27	[60]
*US-Dk1	Grassland	M/Th	Festuca arundinacea Shreb.	2.0	1.0	0.8		0.20	1.03	0.35	0.31	[61]
*US-Dk2	Forest	M/Th/B, D	*Quercus sp., Carya sp., Liquidambar styraciflua* L., *Liriodendron tulipifera* L.	7.0	1.0	25		0.13	1.49	0.36	0.33	[16]
*US-Dk3	Forest	M/Th/N, E	*Pinus taeda* L.	5.3	1.0	18		0.11	0.90	0.41	0.34	[16]
*US-Fuf	Forest	M/Tsd, N, E	*Pinus ponderosa* Douglas ex Laws	2.3	2.0	18		0.10	3.43	0.20	0.50	[63]
*US-Fmf	Forest	M/Tsd, N, E	*Pinus ponderosa* Douglas ex Laws	1.1	1.9	18		0.11	3.06	0.19	0.46	[63]

*US-Fwf	Grassland	M/Tsd, N, E	*Pinus ponderosa* Douglas ex Laws, Bromus tectorum L., Elymus repens (L.) Gould	0.6	1.2	0.5		0.18	2.99	0.19	0.39	[63]
*US-Ne1	Cropland	M/Th	*Zea mays* L.	5.2	1.4	2.9		0.17	1.53	0.35	0.29	[64]
*US-Ne2	Cropland	M/Th	*Zea mays L.* or *Glycine max* (L.) Merr.	5.8 or 5.5	1.4	3.4 or 1		0.18	1.77	0.34	0.33	[64]
*US-Ne3	Cropland	M/Th	*Zea mays L.* or *Glycine max* (L.) Merr.	4.2 or 3	1.3	2.4 or 0.8		0.17	1.89	0.33	0.34	[64]

Table 3. Site pairs used in this study. * indicates site pairs which are part of an experimental set-up.

Land management (LMC)			**Land cover change (LCC)**		
Site Pair	**Year**	**Cover**	**Site Pair**	**Year**	**Cover**
BE-Bra – DE-Hai	2007	Forest – Forest	BE-Bra – NL-Ca1	2007 - 2008	Forest – Grassland
BE-Bra – DK-Sor	2007 - 2009	Forest – Forest	BE-Bra – NL-Hor	2007 - 2009	Forest – Grassland
BE-Bra – NL-Loo	2007 - 2009	Forest – Forest	DE-Hai – NL-Ca1	2004 - 2006	Forest – Grassland
DE-Hai – NL-Loo	2004 - 2006	Forest – Forest	DE-Hai – NL-Hor	2004	Forest – Grassland
DE-Meh - NL-Ca1	2004 - 2006	Grassland – Grassland	DE-Meh - NL-Loo	2004 - 2006	Grassland – Forest
DE-Meh – NL-Hor	2004	Grassland – Grassland	DE-Tha – DE-Meh	2004 - 2006	Forest – Grassland
DE-Wet – DK-Sor	2006	Forest – Forest	DE-Tha – NL-Ca1	2004 - 2006	Forest – Grassland
DE-Wet – NL-Loo	2003 - 2006	Forest – Forest	DE-Tha – NL-Hor	2004	Forest – Grassland
DK-Sor – NL-Loo	2006	Forest – Forest	DE-Wet – NL-Ca1	2004 - 2006	Forest – Grassland
*FR-Aur – FR-Lam	2006 - 2010	Cropland – Cropland	FI-Alk – FI-Jok	2003-2004	Forest – Cropland
NL-Ca1 – NL-Hor	2004	Grassland – Grassland	FR-Aur – FR-Pue	2006	Cropland – Forest
*US-Dk2 – US-Dk3	2004 - 2005	Forest - Forest	FR-Lam – FR-Pue	2006	Cropland – Forest
*US-Fuf – US-Fmf	2005 - 2008	Forest – Forest	FR-Lam – FR-LBr	2005 - 2006	Cropland – Forest
*US-Ne1 – US-Ne2	2001 - 2010	Cropland – Cropland	NL-Ca1 – NL-Loo	2004 - 2006	Grassland – Forest

*US-Ne1 – US-Ne3	2001 - 2010	Cropland – Cropland	*US-Dk1 – US-Dk2	2004 - 2005	Grassland – Forest
			*US-Dk1 – US-Dk3	2004 - 2005	Grassland – Forest
			*US-Fmf – US-Fwf	2005 - 2008	Forest – Grassland
			*US-Fuf – US-Fwf	2005 - 2008	Forest – Grassland

Table 4. List of selected MODIS sites and their characteristics. The coordinates give the center of each 2,500 km² area. LST is the change in MODIS-derived land surface temperature (K), VIS is the change in albedo for the visual wavelengths, NIR is the change in albedo in the near infrared wavelengths and SW is the change in albedo for the shortwave radiation and was calculated as the mean of VIS and NIR. SH is a measure for the spatial heterogeneity of LST that was calculated for 1000 pixel pairs; absolute values of this measure are largely dependent on the number of pairs. Similarity of SH between the test sites and the homogeneous sites suggests that the assumption that within a site, the heterogeneous sites only differed in land cover or land cover change, was acceptable.

Latitude	**Longitude**	**Country**	**Δ(LST)**	**Δ(VIS)**	**Δ(NIR)**	**Δ(SW)**	**SH**	**Description**
Land cover change								
17.81° N	90.90° W	Mexico - Guatemala	1.2	0.00	0.01	0.00	1.5	Cropland-dominated Mexico vs. forest-dominated Guatemala
25.77° S	54.62° W	Argentina - Brazil - Paraguay	4.1	0.03	0.03	0.03	1.6	Forest-dominated Argentina vs. cropland-dominated Brazil and Paraguay
30.00° S	57.41° W	Argentina - Brazil	0.7	0.01	0.02	0.01	3.7	Afforested area in Argentina vs. natural grasslands in Brazil
32.42°S	119.39°E	Australia	-0.9	-0.04	-0.08	-0.06	0.7	Forest dominated vs. cropland dominated along the Rabbit Fence
Land management change								

45.39° N	115.40° E	Mongolia - China	-1.8	-0.04	-0.04	-0.04	2.8	Low grazing intensity in China vs. high grazing intensity in Mongolia
68.84° N	23.87° E	Finland - Norway	-0.5	-0.02	-0.02	-0.02	0.9	Low grazing intensity in Norway vs. high grazing intensity in Finland
50.65° N	24.05° E	Poland-Ukraine	0.1	0.00	0.00	0.00	2.0	Small-scale agriculture in Poland vs. large-scale agriculture and abandonment in Ukraine
47.37° N	123.46° W	USA	2.3	0.03	0.05	0.01	1.9	Intensively managed forest vs. protected natural forest at the border of Olympic National Park
5.12° N	118.45° E	Malaysia	0.7	0.00	0.01	0.00	0.9	Plantation vs. protected natural forest at the border of Tabin Wildlife Reserve
Homogeneous sites								
65.20° N	107.51° E	Russia	-0.4	-0.01	-0.01	-0.01	1.3	Boreal forest (Central Siberian Plateau)
4.38° S	64.39° W	Brazil	0.8	0.00	0.00	0.00	1.3	Tropical forest (Amazon Basin)
43.15° N	92.54° W	USA	0.3	0.00	0.02	0.01	1.4	Cropland (Cornbelt, Iowa)

Table 5. Examples of biophysical effects of land management, grouped by affected variable and/or study.

Description of land management change	Δ(variable)	Source
All other variables being constant, albedo was 0.07, 0.10 or 0.13 for pine, beech or oak forest, respectivly.	0.06 VIS + NIR albedo	[28]
In the US, evergreen coniferous summer albedo ranges between 0.06 to 0.10. For broadleaved deciduous forest, summer albedo ranged between 0.12 and 0.18.	0.02 to 0.12 shortwave albedo	[31]
All other variables being constant, albedo was 0.03 and 0.07 in the visible range and 0.28 and 0.20 in the near infrared range for no management and an intrusive future-tree management, respectively.	0.04 VIS albedo 0.08 NIR albedo	[28]
Site-observations for *Pinus sylvestris* L. along a gradient of increasing LAI from 0 to 11 showed an almost stable BHR albedo and an increase from 0.08 to 0.16 for DHR albedo.	0.00 BHR, white sky albedo 0.08 DHR, black sky albedo	[29]
Albedo declined by 10% over an 150+ year age sequence of Douglas fir and western hemlock in the Pacific North West.	10% shortwave albedo	[89]
Following fire in coniferous forest, summertime albedo increased from 0.05 to 0.12. After about 30 years, it decreased to 0.08 and remained stable.	0.07 albedo first 30 years 0.03 albedo rest of life time	[30]
Summer-time albedo of drained peatland under forest is lower (0.12) than that of an undrained fen (0.14).	-0.02 shortwave albedo	[43]

Increasing grazing intensity reduces albedo due to lower vegetation cover (i.e. bare soil).	-3% shortwave albedo	39
Through a decreased soil water holding capacity, excess tillage resulted in higher albedo values than minimum tillage, 0.15 and 0.12, respectively.	0.03 shortwave albedo	36
Mown compared to unmanaged grassland reduced shortwave albedo through a lower litter layer, LAI and biomass	-0.4 shortwave albedo	40,41,72
In grassland, albedo declines with LAI as $\text{Albedo} = 0.1765\ \text{LAI}^{0.1295}$.	$\text{Albedo} = 0.1765\ \text{LAI}^{0.1295}$	73
Ecosystem water conditions can significantly alter the surface albedo of semiarid grassland through their impact on plant growth and ecosystem conditions.	A variation of 0.1 to 0.8 in shortwave albedo	74
For gravimetric water content increasing from 4 to 32%, albedo decreased from 0.14 to 0.06.	0.08 shortwave albedo	36
Soil fertilisation with biochar increased crop yields and thus decreased the albedo by up to 80% after application. Following tillage, albedo decreased by 20-26% compared to soils without biochar application.	-80 % shortwave albedo	75
Conversion of grassland into greenhouses for tomato production increased the albedo from 0.19 to 0.4.	0.21 increase in shortwave albedo	34
Increasing fertilization improved grassland water use efficiency but increased absolute evapotranspiration, and thus the latent heat flux, from 280 to 310 mm	30 mm evapotranspiration	76

With increasing irrigation from 50 to 350 mm, evapotranspiration increased from 460 to 650 mm but saturated at 650 mm for 150 mm of irrigation.	190 mm evapotranspiration	[35]
Species conversion from pine to hardwood forest results in a sustained decrease in streamflow of ~200 mm/year for sites experiencing similar precipitation (i.e., the majority of the difference reflects differences in ET)	-200 mm/year streamflow	[77]
Coppice management of a southern Appalachian hardwood forest resulted in a sustained decrease in streamflow of ~75 mm/year when compared to an unmanaged control. Sites experienced similar precipitation (i.e., the majority of the difference reflects differences in ET).	-75 mm/year streamflow	[77]
Water-level drawdown of >60 cm decreased evapotranspiration in a pristine bog; similar behaviour could be expected after drainage.	Evapotranspiration (mm d^{-1}) = -0.08 * WT (cm) + 6.9	[78]
In drained peat soil, ET in dry years depends on soil hydraulic properties, in wet years on the evaporative demand by the atmosphere.	n.a.	[46]
Drops in the ground water level below 0.3 m significantly decreased evapotranspiration in a wet spruce forest (RU-Fyo); similar behavior is to be expected after forest drainage.	50% decrease in summer evaporation	Personal communication Andrej Varlagin
Restoration of a peat-harvesting area back to natural peatland decreased evapotranspiration.	10% decrease in growing season evapotranspiration	[79]

Compared to bare soil, crop residues reduced extremes of heat and mass fluxes at the soil surface.	>10 K difference in top of the soil temperatures at midday	37
Earlier planting has led to an increase in the latent heat flux (7.3 mm or 7.1 Wm^{-2}) and a decrease in the sensible heat flux (5.7 Wm^{-2}) in June, although annual changes are small.	7.3 mm or 7.1 Wm^{-2} latent heat -5.7 Wm^{-2} sensible heat	38
Logging of tropical forest decreasing canopy coverage from 96 to 88% resulted in an increase of 1 to 2 Wm^{-2} in sensible heat flux and decrease of 3 to 4 Wm^{-2} in latent heat flux.	1 to 2 Wm^{-2} sensible heat -3-4 Wm^{-2} (latent heat)	80
A shorter time for crops from crops maturity to harvest has meant an increase in net radiation in October (2.7 Wm^{-2}).	2.7 Wm^{-2} net radiation	38
Decrease in summer season night-time temperature, particularly during clear nights, due to the drainage of peatland	Up to -10 K surface temperature	81
Irrigation has cooled the global surface by about 0.8 K.	-0.8 K surface temperature	82
Despite its surface cooling, irrigation was simulated to increased global radiative forcing in the range of 0.03 to 0.1 Wm^{-2}.	0.03 to 0.1 Wm^{-2} top of the atmosphere radiative forcing	82
Afforestation of dryland shrubland to open-canopy pine forest. A large sensible heat flux over the forest effectively shifts heat from the surface to the lower atmosphere. Net shortwave radiation increased by +24 Wm^{-2}, albedo decreased by 0.1, the canopy	24 Wm^{-2} shorwave radiation -0.1 shortwave albedo -5 K surface temperature	15

temperature increased 3 K, the surface temperature decreased by 5 K and the outgoing longwave radiation decreased by 25 Wm^{-2}.	3 K below-canopy temperature -25 Wm^{-2} outgoing longwave radiation	
Compared with an undisturbed forest, an intensely burned forest had 30% higher albedo, lower latent and sensible heat fluxes, greater soil heat flux, a slower soil water depletion and warmer surface soil in summer by 3 to 7 K	0.04 to 0.05 shortwave albedo 3 to 7 K surface temperature	83
Afforestation of old grass field to pine plantation caused albedo to decrease by 0.08, and an increase in evapotranspiration of ~100 mm per year.	-0.08 shortwave albedo 100 mm evapotranspiration	16
Afforestation of old grass field to deciduous hardwood forest caused albedo to decrease by 0.03, and an increase in evapotranspiration of ~55 mm per year.	-0.03 shortwave albedo 55 mm evapotranspiration	16
Changing tree density of Mediterranean-type ecosystems dominated by the evergreen *Quercus ilex* from shrubland with tree cover <25% to dense forest (75%<Tree cover<100%) yielded a decline of albedo by 12 to 15% and a decrease in surface temperature by ca. 3.5 K, regardless of date from early May to late September	-12 to -15% shortwave albedo -3.5 K surface temperature	84
In a mulching experiment net radiation was 20% lower for crops with mulch compared to bare soil, the sensible heat flux was 100 Wm^{-2} for bare soil compared to 400 Wm^{-2} for mulch, the latent heat was 500 Wm^{-2} for bare soil compared to 350 Wm^{-2} for mulch and the soil heat flux was 200 Wm^{-2} for bare soil compared to 75 Wm^{-2} for the	-20% net radiation 300 Wm^{-2} sensible heat -150 Wm^{-2} latent heat -125 Wm^{-2} soil heat flux	85

mulched treatment		
For two maize hybrids albedo increased by 3.9% and 13.5% from thin to normal/dense packing, respectively. H varied from 55 to 189.5 Wm^{-2} for cultivar 1 and from 41.5 to 170.15 Wm^{-2} for cultivar 2 for thin to dense packing, respectively. λE varied from 224 to 259.8 Wm^{-2} for cultivar 1 and from 248 to 281.6 Wm^{-2} for cultivar 2 for thin to dense packing, respectively.	3.9% to 13.5% shortwave albedo 14 to 19 Wm^{-2} sensible heat 22 to 24 Wm^{-2} latent heat	[86]
Excluding grazing by bison in the Great Plains induced cooling in T_{max} and warming in T_{min}		[87]
Site comparison of a one-year-old harvest of aspen/poplar compared to a mature forest resulted in 13% decrease of the net radiation, a 45% decrease in sensible heat and a 54% decrease in latent heat.	-13% net radiation -45% sensible heat flux -54% latent heat flux	[88]

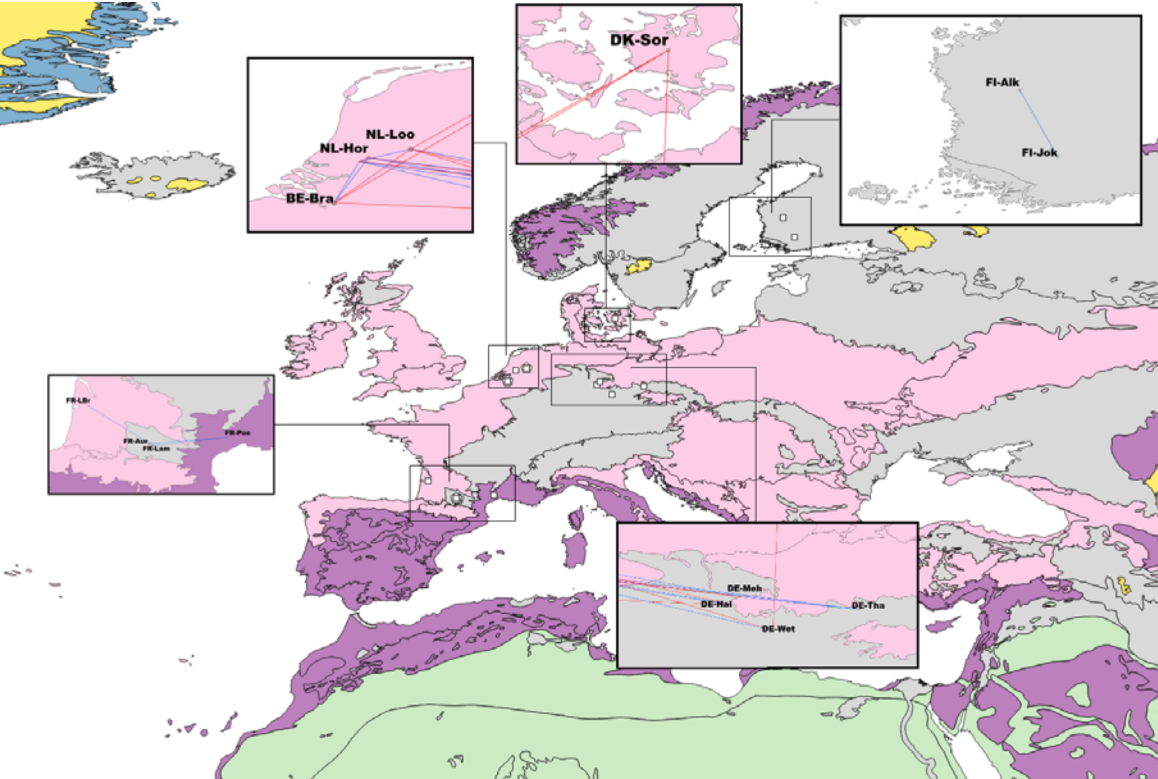
DK-Sor
FI-Alk
FI-Jok
NL-Loo
NL-Hor
BE-Bra
FR-LBr
FR-Pue
FR-Aur
FR-Lam
DE-Meh
DE-Hai
DE-Tha
DE-Wet

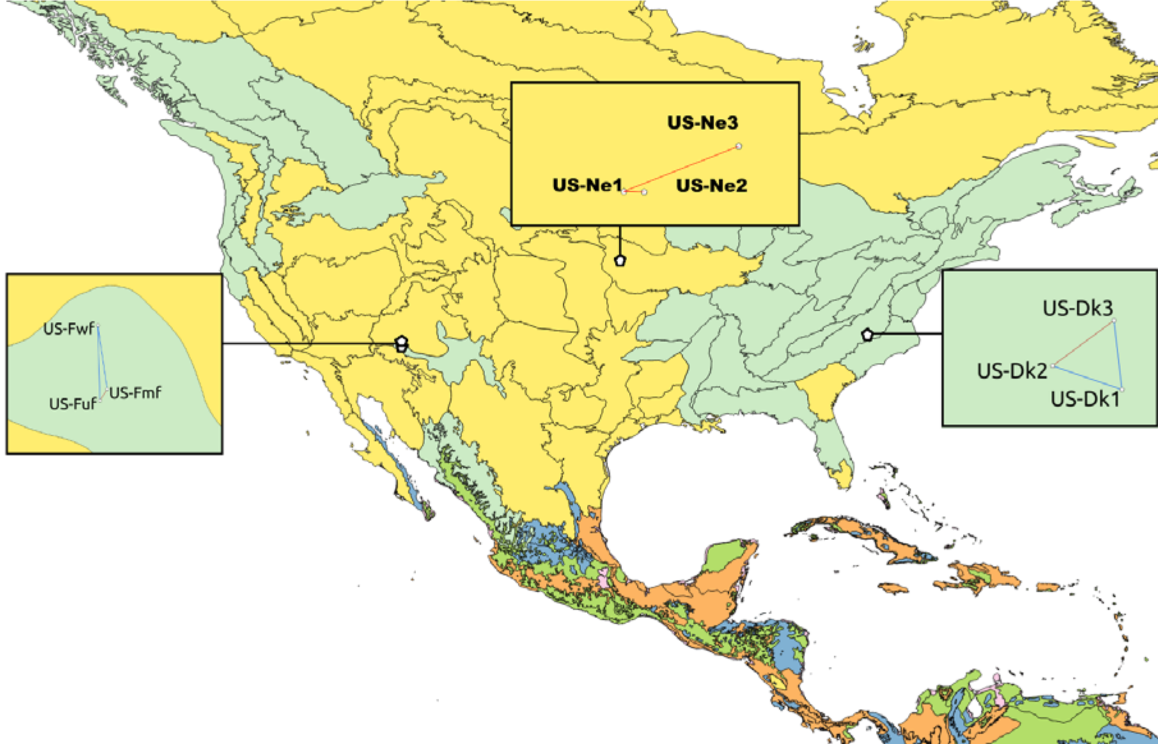
US-Ne3
US-Ne1
US-Ne2
US-Fwf
US-Fmf
US-Fuf
US-Dk3
US-Dk2
US-Dk1

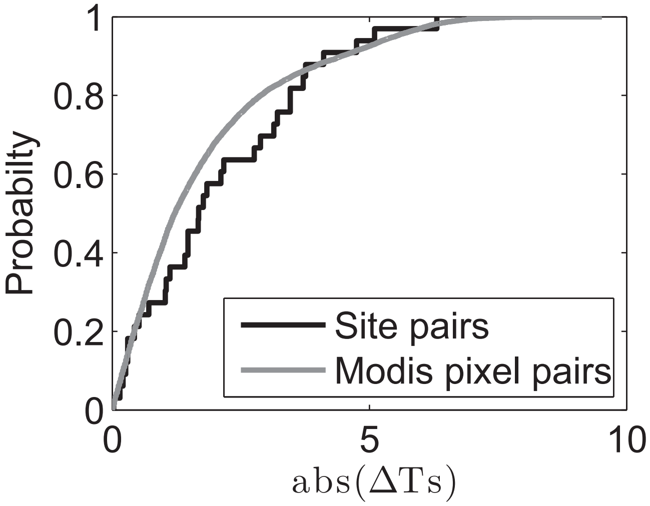
1
0.8
0.6
0.4
0.2
0
Probabilty
0
5
10
abs(ΔTs)
Site pairs
Modis pixel pairs

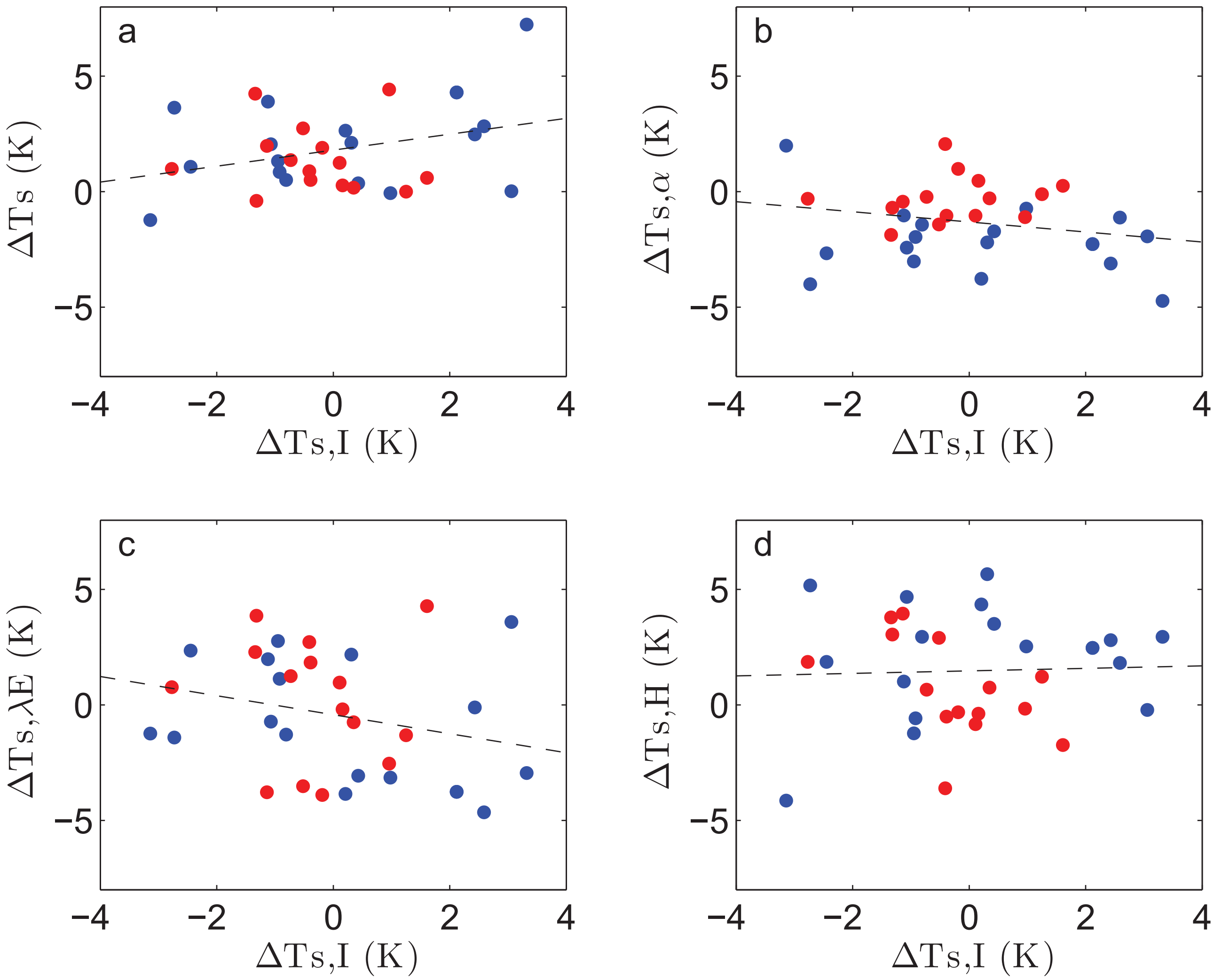
a
b
c
d
ΔTs (K)
ΔTs,α (K)
ΔTs,λE (K)
ΔTs,H (K)
ΔTs,I (K)
5
0
−5
−4
−2
0
2
4

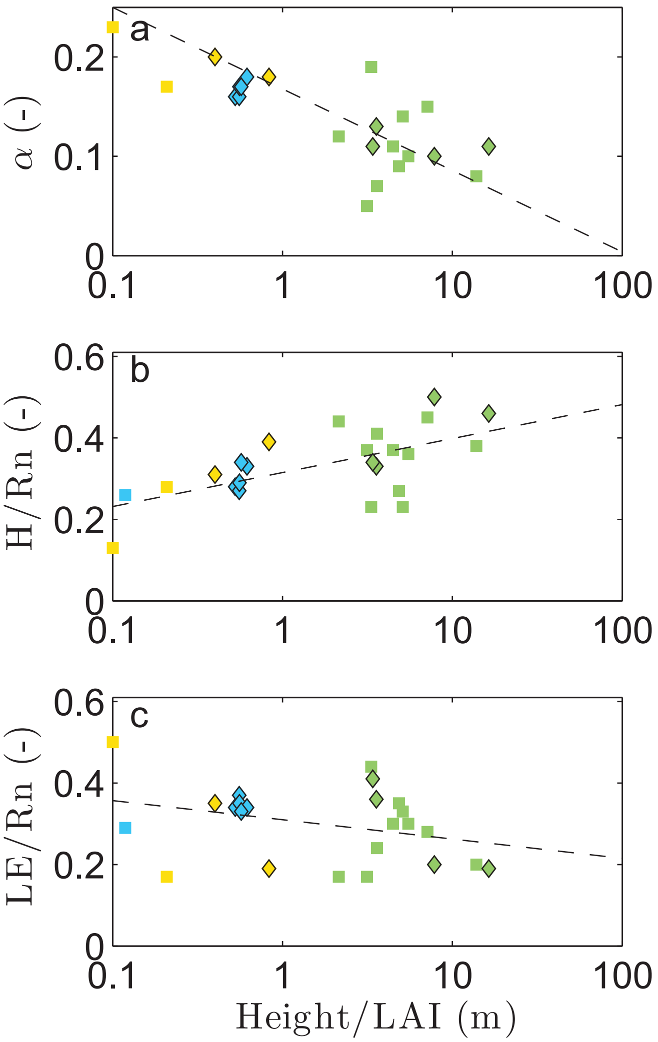
a
α (-)
0.2
0.1
0
0.1
1
10
100
b
H/Rn (-)
0.6
0.4
0.2
0
0.1
1
10
100
c
LE/Rn (-)
0.6
0.4
0.2
0
0.1
1
10
100
Height/LAI (m)